

ADAPTIVE ROBUST CONTROL FOR SIX-DEGREE-OF-FREEDOM ELECTRO-HYDRAULIC PARALLEL SHIP STABILIZATION PLATFORM

Jing Chenghu^{1*}[0000-0001-5333-4651], Ma Xiaole¹, Du Haohao¹, Liu Yafeng¹, Liu Chunbo¹, Hui Yanbo¹
¹*School of Mechanical and Electrical Engineering, Henan University of Technology, Zhengzhou 450001, China*
*Corresponding author: Jing Chenghu
Email: chhjing@haut.edu.cn

Abstract - Stewart is a classic six degree of freedom parallel mechanism widely used in various situations. This paper investigates the dynamic model and control of the Stewart mechanism as a ship stability platform. Stewart stability platform faces significant challenges due to continuous and unpredictable disturbances from ocean waves and other environmental factors under harsh sea conditions. This paper develops a nonlinear model of the asymmetric hydraulic system of a 6-DOF Stewart stabilization platform and proposes an adaptive robust control method for shipboard stabilization platforms. Using Lyapunov function theory, the stability of the system is analyzed and proven. The proposed adaptive robust control method combines backstepping recursive design with sliding mode control and robust adaptive laws to enhance the platform's anti-disturbance capability and control accuracy. A control system model is built, and simulations are conducted to evaluate the performance of the Stewart stabilization platform under various control algorithms in the presence of ship motion disturbance. Simulation results demonstrate that the proposed control method improves tracking performance and robustness, making it well-suited for stabilizing a Stewart platform under complex sea conditions.

Keywords: Ship stabilization platform; Stewart; Robust adaptive control; Hydraulic system; sliding mode control; Lyapunov function.

1. Introduction

Maritime operations are significantly impacted by weather and sea conditions, with ships often subjected to complex environmental factors such as wind, waves, and tides, which lead to coupled motions [1]. These not only severely affect operational efficiency, causing economic losses but also greatly compromise safety. The six-degree-of-freedom (6-DOF) parallel mechanism, as a type of ship stabilization platform, boasts advantages including high stiffness, strong load-bearing capacity, excellent dynamic performance, and full-DOF compensation [2,3]. It can monitor the multi-dimensional motion of the ship relative to the inertial coordinate system in real-time and actively compensate for disturbances through control algorithms, effectively ensuring the relative stability of equipment and person, thereby safeguarding human-machine safety [4].

Salzmann [5] proposed the idea of using the Stewart platform as a motion compensation system. However, the Stewart stabilization platform is a nonlinear, strongly coupled complex system [6,7]. This poses a great challenge to the high-precision position tracking control of the Stewart platform.

To improve its control accuracy, some advanced algorithms have been applied to the Stewart platform, such as adaptive control, sliding mode control, intelligent control, and so on. The control method of static (inertial) Stewart platform has been widely studied and has achieved fruitful results, such as sliding mode control [8-10], adaptive control [11], inverse dynamics control [12], observer-based control [13], reinforcement learning-based control [14] and so on. Unlike the Stewart in an inertial coordinate system where the lower platform is fixed [15], the Stewart ship stabilizing platform belongs to a parallel mechanism in a non-inertial frame [16]. In addition to Stewart's inherent nonlinearity and coupling characteristics, the stable platform of a ship under non inertial conditions is affected by ship motion, mainly manifested as motion coupling between the upper platform and the ship, as well as force disturbances caused by ship entrainment motion. All of these will affect the accuracy of ship motion compensation on the platform. At present, there is not much research on control methods for parallel mechanisms in non-inertial frames, especially in the field of wave or ship motion compensation.

In order to improve the accuracy of wave compensation, researchers have made a lot of efforts

in control. Qiang [17] proposed a model predictive control strategy for ship stabilization platforms based on an autoregressive predictive model, which showed better control performance compared to traditional model predictive control strategies. However, model predictive control is highly sensitive to the model. Sliding mode control is a robust control that is insensitive to models and disturbances. Chen [18] integrated an internal model controller, sliding mode controller, and active disturbance rejection control to develop a control method for the ship-mounted Stewart platform, which was demonstrated that the proposed control strategy excels in power reduction, decoupling control, and disturbance rejection. He also investigated the modal space proportional and derivative control and the modal space sliding mode controller for ship-borne Stewart platform [19], which improved the wave compensation rate. However, these works [18,19] are aimed at electric-driven ship-mounted Stewart platform. For electro-hydraulic Stewart stabilization platform, Cai [20] analyzed its model and proposed a sliding mode control scheme based on velocity feedback compensation. On this basis, they further combined adaptive control methods to design an adaptive robust dual loop control scheme, and demonstrated through simulation results that these control methods achieved good wave compensation effects [21]. However, these works considered the hydraulic system model and its uncertainty, but did not take into account the unmodeled dynamics of the hydraulic system.

Due to the strong robustness and fast response advantages of sliding mode control [22,23], the aforementioned work applied this method to stabilize the platforms. It can be inferred that sliding mode control is a promising control approach. However, one significant drawback of sliding mode control is the presence of chattering. Thus, this paper proposes an adaptive robust control for stabilizing the platform. Utilizing backstepping design, the virtual control relies on adaptive sliding mode control to adaptively reduce the uncertainties associated with the mechanical system parameters. The actual control rate employs adaptive sliding mode control based on immersion and invariance approach to estimate and counteract the unmodeled dynamics and parameter uncertainties of the hydraulic system. Through adaptive means and sliding mode control, the aim is to reduce chattering, enhance the system's robustness, and improve the stabilization effect of the platform.

2. Principles and Mathematical Models

The stabilized platform studied in this paper is based on the standard Stewart mechanism, where the upper platform is connected to the base platform through six legs. To enhance the load bearing capacity of the

parallel mechanism, the actuators are connected to both platforms using Hooke joints. The upper platform is used to carry the stabilized object, while the base platform is fixed to the hull and moves with the ship. As shown in Figure 1, the stabilized platform is installed on the deck of the ship, and the ship's motion is measured by a 6-DOF IMU. The continuously detected ship's pose is transmitted to the control system, which compensates for the disturbances caused by the hull's motion by controlling the extension and retraction of the hydraulic actuators, thereby stabilizing the upper platform relative to the inertial reference frame.

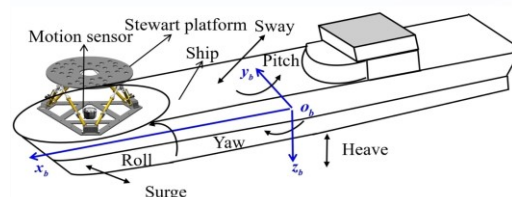


Figure 1: Ship-mounted Stewart Platform

To facilitate the description of the dynamic model of the mechanical system of the stabilized platform, three coordinate systems are established as shown in Figure 2:

- (1) Ship-fixed frame O_b-x_b, y_b, z_b , attached to the ship, with the origin O_b located at the center of the motion sensor. In this frame, the x_b points towards the bow of the ship, which is also the direction of the ship's forward motion, and the z_b is perpendicular to the deck.
- (2) Platform-fixed frame O_p-x_p, y_p, z_p , attached to the upper platform of the Stewart mechanism, with its origin O_p located at the center of the upper hinge points. In the neutral position, the orientations of its axes are parallel to the corresponding axes in the ship-fixed frame.
- (3) Inertial frame of reference O_0-x_0, y_0, z_0 , fixed to the ground. At the initial position, the coordinate axes of the inertial frame and the ship-fixed frame have the same orientation.

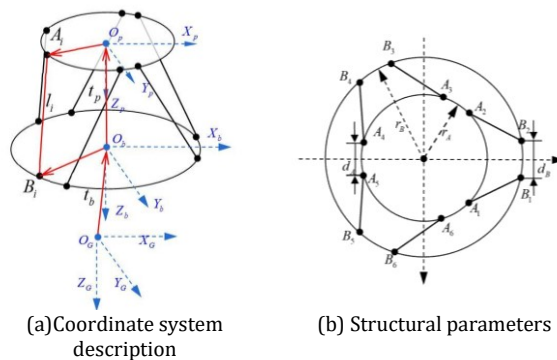


Figure 2: Coordinate Systems and Structural Parameters

To analyze the dynamic characteristics of a ship stability platform, it is first necessary to mathematically describe the state of the ship. This involves defining the generalized coordinates $\mathbf{q}_b = (\psi_b, \theta_b, \varphi_b, x_b, y_b, z_b)^T$ of the origin \mathbf{O}_b , where $\mathbf{t}_b = (x_b, y_b, z_b)^T$ represents the position vector in the inertial frame of reference. Additionally, the orientation of the ship relative to the inertial frame can be described using the following Euler transformation matrix:

$$\mathbf{R}_{gb} = \begin{bmatrix} c\psi c\theta & c\psi s\theta c\varphi - s\psi c\varphi & s\psi s\varphi + c\psi s\theta c\varphi \\ s\psi c\theta & c\psi c\varphi + s\psi s\theta s\varphi & s\psi s\theta c\varphi - c\psi s\varphi \\ -s\theta & c\theta s\varphi & c\theta c\varphi \end{bmatrix} \quad (1)$$

where $s \cdot = \sin(\cdot)$ and $c \cdot = \cos(\cdot)$, the definitions will remain consistent throughout the following text.

Similarly, in a stable platform system, let \mathbf{O}_p be the origin of the generalized coordinates $\mathbf{q}_p = (\psi_p, \theta_p, \varphi_p, x_p, y_p, z_p)^T$ of the platform, and let $\mathbf{t}_p = (x_p, y_p, z_p)^T$ be the position vector of the upper platform relative to the ship-fixed frame. The orientation of the upper platform relative to the ship-fixed frame can be described using an Euler transformation matrix \mathbf{R}_{bp} .

2.1. Kinematic Model

The inverse solution for a parallel mechanism involves determining the extension lengths of the hydraulic actuators given the spatial pose of the ship-fixed frame. From the spatial vector relationship shown in equation (2), the coordinate transformation relationship between the upper and lower hinges can be derived.

$$\mathbf{l}_i = \mathbf{t}_p + \mathbf{R}_{bp} \mathbf{A}_i - \mathbf{B}_i \quad (2)$$

where \mathbf{A}_i is the coordinates of the upper hinges in the platform-fixed frame, \mathbf{B}_i is the coordinates of the lower hinges in the ship-fixed frame.

Thus, for the platform to move from its current position to the desired position, the extension amounts of the hydraulic actuators are given by:

$$\Delta \mathbf{l}_i = \mathbf{l}_i - \mathbf{l}_i' \quad (3)$$

where \mathbf{l}_i' is the current length of the hydraulic cylinders; if the platform starts moving from the initial position, then $\mathbf{l}_i' = \mathbf{l}_0$.

The matrix form of the velocities of the six hydraulic actuators is:

$$\dot{\mathbf{l}} = \begin{bmatrix} \mathbf{L}_n^T & -(\mathbf{R}_{bp} \mathbf{A}_i^p \times \mathbf{L}_n)^T \end{bmatrix} \begin{bmatrix} \dot{\mathbf{t}}_p \\ \boldsymbol{\omega}_{pb} \end{bmatrix} = \mathbf{J} \dot{\mathbf{q}}_p \quad (4)$$

where \mathbf{J} is the Jacobian matrix relating the velocity of the upper platform to the extension velocities of the hydraulic actuators, $\dot{\mathbf{q}}_p$ is the velocity of the center of mass of the upper platform in the static coordinate system, \mathbf{L}_n is the unit vector matrix of the hydraulic actuators.

2.2. Dynamic Model

To reduce computational complexity and facilitate programming, we established a dynamic model using Kane's method. Here, inertial forces, inertial moments, gravitational forces, and driving forces are projected into task space through the Jacobian matrix as generalized inertial forces and generalized driving forces. The dynamic equations of the ship-mounted stable platform can be expressed as:

$$\mathbf{M}_p \ddot{\mathbf{q}}_p + \mathbf{C}_p \dot{\mathbf{q}}_p - \mathbf{G}_p + \mathbf{M}_b \ddot{\mathbf{q}}_b + \mathbf{C}_b \dot{\mathbf{q}}_b = \mathbf{J}^T \mathbf{f}_a \quad (5)$$

where \mathbf{M}_p is the relative motion mass matrix of the ship-mounted stable platform, \mathbf{C}_p is the relative motion centrifugal force/Coriolis force matrix of the ship-mounted stable platform, \mathbf{G}_p is the gravity term of the ship-mounted stable platform, \mathbf{M}_b is the coupled mass matrix of the stable platform and ship motion, \mathbf{C}_b is the coupled centrifugal force/Coriolis force matrix of the stable platform and ship motion, \mathbf{f}_a is the actuator driving force vector.

Equation (5) describes the inertial forces due to the relative motion of the ship-mounted stable platform with respect to the ship in the first two terms on the left side, and the coupling between the stable platform and the ship's motion in the last two terms. The difference from a statically-based six-degree-of-freedom(6-DOF) parallel platform lies in this coupling. Therefore, the driving forces generated by the actuators are first transformed by the system Jacobian matrix and then divided into three parts: the first part drives the inertial forces due to relative motion, the second part drives the inertial forces due to the coupled motion, and the third part overcomes gravity, which is influenced by the ship's pose.

Since displacement sensors are generally installed on the actuators, to facilitate controller design, both sides of Equation (5) are multiplied on the left by \mathbf{J}^T , resulting in the joint space dynamic equation:

$$\mathbf{M}_i \ddot{\mathbf{l}} + \mathbf{C}_i \dot{\mathbf{l}} - \mathbf{G}_i + \mathbf{M}_c \ddot{\mathbf{q}}_b + \mathbf{C}_c \dot{\mathbf{q}}_b = \mathbf{f}_a \quad (6)$$

2.3. Valve-controlled Asymmetric Cylinder Model

To meet the requirements of high load, multi-degree-of-freedom stability, and harsh sea conditions in practical applications, the dynamic platform is driven by valve-controlled hydraulic actuators. Since the structure of all six actuators is identical, modeling one actuator serves as a representative example. The schematic diagram of the hydraulic actuator driver is shown in Figure 3.

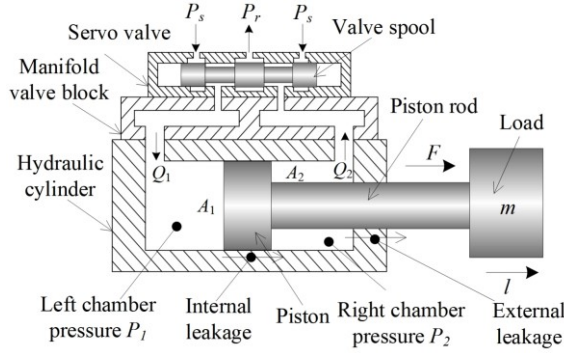


Figure 3: Schematic of hydraulic actuator

In Figure 3, P_1 and P_2 represent the pressure in the two chambers of the hydraulic cylinder; A_1 is the piston area, A_2 is area of the piston rod; Q_1 and Q_2 are the flow rates into and out of the hydraulic cylinder (m^3/s), respectively; l is the actuator's displacement (m), P_s is oil source pressure (Pa), P_r is back pressure (Pa).

The dynamic equation of the hydraulic actuator is written as:

$$\dot{P}_L = \frac{(1+n_0^2)\beta_e}{V_0} (K_0 f(\bar{p}_L)u - A_1 \dot{l} - C_{lc} P_L) + \Delta \quad (7)$$

where K_0 is constant, $K_0 = C_d w k_v \sqrt{2P_s / [\rho(n^3+1)]}$; β_e is effective bulk Elastic Modulus of hydraulic Oil (Pa); C_{lc} is equivalent leakage coefficient ($\text{m}^3/\text{s}/\text{Pa}$), C_d is slide valve flow coefficient ($\text{m}^3/\text{s}/\text{Pa}$), w is slide valve area gradient, k_v is voltage signal gain coefficient, ρ is fluid density (kg/m^3), u is input voltage signal of servo valve control system, V_0 is the initial control volume of hydraulic actuator (m^3); $f(\bar{p}_L)$ is servo valve flow nonlinearity, $f(\bar{p}_{il}) = \begin{cases} \sqrt{1-\bar{p}_{il}}, u_i \geq 0 \\ \sqrt{n_0 + \bar{p}_{il}}, u_i < 0 \end{cases}$, $\bar{p}_L = \frac{P_L}{P_s}$, $f(\bar{p}_L) = \text{diag}\{f(\bar{p}_{1L}), f(\bar{p}_{2L}), \dots, f(\bar{p}_{6L})\}$, Δ represents the aggregate uncertainty including parameter uncertainty and unmodeled dynamics.

The above model is aimed at the hydraulic drive system of each leg. Considering the overall dynamic model, equation (6) can be written as

$$M_l \ddot{l} + C_l \dot{l} - G_l + M_G \ddot{q}_b + C_G \dot{q}_b = f_p = P_L A_1 \quad (8)$$

The models described by Equations (7) and (8) are utilized to design the control system of the shipborne stabilization platform. The joint space control method is adopted to simplify the control model block diagram as shown in Figure 4.

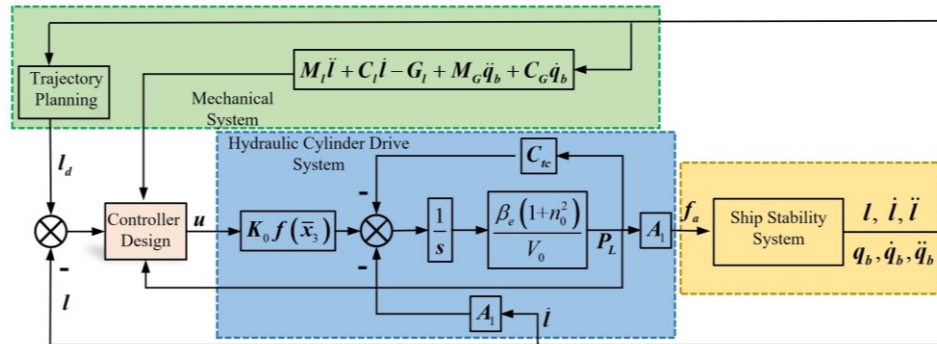


Figure 4: Simplified control model block diagram

To summarize, the state variable is defined as $x = [x_1, x_2, x_3]^T = [l^r, \dot{l}^r, P_L^r]^T$, and the entire system, including mechanical subsystem (moving platform) and hydraulic subsystem (electro-hydraulic servo actuator), can be expressed in the form of state space as:

$$\dot{x}_1 = x_2 \quad (9)$$

$$M_l \dot{x}_2 = A_1 x_3 - C_l x_2 + G_l - (M_G \ddot{q}_b + C_G \dot{q}_b) \quad (10)$$

$$\dot{x}_3 = (1+n_0^2)\beta_e (K_0 f(\bar{x}_3)u - A_1 x_2 - C_{lc} x_3) / V_0 + \Delta \quad (11)$$

The whole system model satisfies the properties and basic assumptions of the following general mechanical system models [20,21]:

Assumption 1: The ship motion information $q_b, \dot{q}_b, \ddot{q}_b$ is bounded, i.e. $q_b, \dot{q}_b, \ddot{q}_b \in L_\infty$.

Assumption 2: The stable platform is installed on a large ship, and it is assumed that the motion of the

stable platform relative to the ship will not affect the motion of the ship.

Assumption 3: the definition of interference Δ and its first derivative $\dot{\Delta}$ are bounded, and there are positive numbers δ_{i1} and δ_{i2} such that $|\Delta_i| \leq \delta_{i1}$ and $|\dot{\Delta}_i| \leq \delta_{i2}$ hold.

Property 1: The mass matrix M_I is a symmetric and positive definite. Therefore, the following inequality holds true

$$m_1 \|\zeta\|^2 \leq \zeta^T M_I \zeta \leq m_2 \|\zeta\|^2, \forall \zeta \in R^6 \quad (12)$$

Property 2: since the mass matrix and the centrifugal force-Coriolis force matrix are only related to the posture of the upper platform relative to the foundation platform, similar to the static foundation six-degree-of-freedom platform, the mass matrix M_I and the centrifugal force / Coriolis force matrix C_I have a skew-symmetric relationship, as shown in the following equation:

$$\zeta^T (\dot{M}_I / 2 - C_I) \zeta = 0, \forall \zeta \in R^6 \quad (13)$$

2.4. Control Task

The position vector of the upper platform remains unchanged. Considering that the motion sensor is not installed on the upper platform, the goal can be achieved by controlling the length of the actuator. For this reason, first, according to the ship motion measured by the motion sensor, the relative motion trajectory of the upper platform with respect to the ship is determined, and then the expected length required by the actuator is calculated, as shown below.

$$l_d = \|\dot{t}_p + R_{bp} A_i - B_i\| \quad (14)$$

Therefore, the design goal of the controller is to develop a bounded control system to input voltage signal u in the case of ship motion disturbance, so that the actual length of the hydraulic actuator can quickly and stably track the desired length l_d .

3. Controller Design and Stability Analysis

Given that the six-degree-of-freedom ship stabilization platform is a nonlinear time-varying system, the recursive backstepping control method is used to design the controller, and the complex ship stability control system is decomposed into several lower-order subsystems. The Lyapunov function and virtual controller can be selected separately for each subsystem to stabilize each subsystem model, so the

control signal can be flexibly selected to improve the control system energy. Next, we will employ the concept of backstepping control to construct the entire control strategy framework. To achieve the design of the controller, we decompose the entire system into two subsystems: the mechanical subsystem model represented by Equations (9) and (10) is considered as the first lower-order subsystem, while the hydraulic subsystem model represented by Equation (11) is treated as the second lower-order subsystem, and x_{3d} is assumed to be a virtual control quantity.

Step1: Define subsystem tracking error $\tilde{x}_1 = x_1 - x_{1d}$, where $x_{1d} = l_d$. A sliding mode surface is designed as

$$s = \dot{\tilde{x}}_1 + \lambda_1 \tilde{x}_1 + \lambda_2 \int \tilde{x}_1 dt \quad (15)$$

where λ_1 and λ_2 are positive definite matrices. Furthermore, the auxiliary vector η is defined as

$$\eta = \lambda_1 \tilde{x}_1 + \lambda_2 \int \tilde{x}_1 dt - \dot{x}_{1d} \quad (16)$$

It can be seen that if the above sliding mode surface is stable, making s converge to 0 or be bounded is equivalent to making the tracking error vector \tilde{x}_1 converge to 0 or bounded to meet the requirements of the control target.

The first step is to transform the mechanical system dynamics equation of the shipborne stabilization platform into an error model based on sliding mode surface. The goal of this subsystem is to determine the virtual control rate x_{3d} to make s as small as possible.

From equation (9), it follows that

$$\tilde{x}_2 = x_2 - \dot{x}_{1d} \quad (17)$$

Differentiating equation (19) yields

$$\dot{\tilde{x}}_2 = \dot{x}_2 - \ddot{x}_{1d} \quad (18)$$

Using equation (18), differentiating equation (15) yields

$$\dot{s} = \dot{x}_2 - \ddot{x}_{1d} + \lambda_1 \dot{\tilde{x}}_1 + \lambda_2 \tilde{x}_1 \quad (19)$$

Using equation (10), equation (16) and equation (19), one obtains

$$M_I \dot{s} = A_1 x_3 - C_I s + (M_I \dot{\eta} + C_I \eta + G_I - M_G \ddot{q}_b - C_G \dot{q}_b) \quad (20)$$

x_1 and x_3 can be regarded as the output and virtual input of the first subsystem, respectively. In

order to enable the system torque output x_1 to track the expected torque x_{1d} , it is necessary to design a virtual control law x_{3d} for the virtual input x_3 , and define $\tilde{x}_3 = x_3 - x_{3d}$ controllers. In order to analyze the stability, the following Lyapunov functions are selected for the first-level subsystem.

$$V_s = s^T M_1 s / 2 \quad (21)$$

Considering property 2, the derivation of Lyapunov function V_s is obtained as

$$\dot{V}_s = s^T (A_1 x_{3d} - C_1 s + (M_1 \dot{\eta} + C_1 \eta + G_1 - M_c \ddot{q}_b - C_c \dot{q}_b)) + \tilde{x}_3^T A_1 s \quad (22)$$

According to the above equation, the virtual control law x_{3d} is designed.

$$x_{3d} = \frac{1}{A_1} (\varphi_R(q, \dot{q}) \theta - k_1 s - k_2 \tanh(s_1)) \quad (23)$$

where

$\varphi_R(q, \dot{q}) \theta = C_1 s - (M_1 \dot{\eta} + C_1 \eta + G_1 - M_c \ddot{q}_b - C_c \dot{q}_b)$, k_1 and k_2 are the control gains of the dynamic surface controller and are positive definite matrices.

Substituting equation (23) into equation (22), the Lyapunov function V_s is rewritten as

$$\dot{V}_s = -s^T k_1 s + s^T k_2 \tanh(s) + \tilde{x}_3^T A_1 s \quad (24)$$

Step 2: According to the Lyapunov stability theory, if the system is to be stable, it is necessary to ensure $\dot{V}_s < 0$, so the next step is to design a suitable real control rate u , so that the x_3 tracking x_{3d} is as close as possible, that is, \tilde{x}_3 close to 0.

The derivative of the state \tilde{x}_3 is written as

$$\begin{aligned} \dot{\tilde{x}}_3 &= \frac{(1+n_0^2)\beta_e}{V_0} (K_0 f(\bar{x}_3) u - A_1 x_2 - C_{tc} x_{3u}) \\ &\quad - \frac{(1+n_0^2)\beta_e}{V_0} \dot{x}_{3d} + \frac{(1+n_0^2)\beta_e}{V_0} \dot{A}_u \end{aligned} \quad (25)$$

where $\dot{A}_u = \frac{V_0}{(1+n_0^2)\beta_e} \dot{A}$.

Using \hat{A}_u as an estimate of A_u , the control law u is designed as follows:

$$\begin{aligned} u &= \frac{1}{K_0 f(\bar{x}_3)} \left(A_1 x_2 + C_{tc} x_3 + \frac{V_{10}}{(1+n_0^2)\beta_e} \dot{x}_{3d} \right) \\ &\quad - \frac{1}{K_0 f(\bar{x}_3)} \left[\rho_1 \varphi(\tilde{x}_3) + (\hat{A}_u + \beta(\tilde{x}_3)) \right] \end{aligned} \quad (26)$$

where ρ_1 is the control gain of the dynamic surface controller and is a positive constant matrix. $\varphi(\tilde{x}_3) = \gamma \tilde{x}_3 - \text{sign}^{0.5}(\tilde{x}_3)$, $\gamma > 0$ is a constant, $\text{sign}^{0.5}(\tilde{x}_3) = \left[|\tilde{x}_{31}|^{0.5} \text{sign}(\tilde{x}_{31}), \dots, |\tilde{x}_{36}|^{0.5} \text{sign}(\tilde{x}_{36}) \right]^T$.

The adaptive control rate is designed, and the estimation error of \hat{A}_u is defined as

$$\varepsilon = \hat{A}_u + \beta(\tilde{x}_3) - A_u \quad (27)$$

Substituting equations (26) and (27) into equation (25), one obtains

$$\dot{\tilde{x}}_3 = -\rho_1 \varphi(\tilde{x}_3) + \varepsilon \quad (28)$$

From equation (25), the derivative of the estimation error ε is written as

$$\begin{aligned} \dot{\varepsilon} &= \dot{\hat{A}}_u - \dot{A}_u + \frac{\partial \beta}{\partial \tilde{x}_3} \dot{\tilde{x}}_3 \\ &= \dot{\hat{A}}_u + \frac{(1+n_0^2)\beta_e}{V_{10}} \frac{\partial \beta}{\partial \tilde{x}_3} (K_0 f(\bar{x}_3) u - A_1 x_2 - C_{tc} x_3) \\ &\quad + \frac{(1+n_0^2)\beta_e}{V_{10}} \frac{\partial \beta}{\partial \tilde{x}_3} \left(-\frac{V_{10}}{(1+n_0^2)\beta_e} \dot{x}_{3d} + \dot{A}_u \right) - \dot{A}_u \end{aligned} \quad (29)$$

Using equation (26), equation (29) is reorganized as

$$\dot{\varepsilon} = \dot{\hat{A}}_u - \dot{A}_u + \frac{\partial \beta}{\partial \tilde{x}_3} \left(-\rho_1 \gamma \tilde{x}_3 - \rho_1 |\tilde{x}_3|^{\frac{1}{2}} \text{sign}(\tilde{x}_3) - \varepsilon \right) \quad (30)$$

The adaptive law of \hat{A}_u is designed as

$$\dot{\hat{A}}_u = \frac{\partial \beta}{\partial \tilde{x}_3} \left(\rho_1 \gamma \tilde{x}_3 + \rho_1 |\tilde{x}_3|^{\frac{1}{2}} \text{sign}(\tilde{x}_3) \right) \quad (31)$$

Using equation (31), equation (30) is further written as

$$\dot{\varepsilon} = -\frac{\partial \beta}{\partial \tilde{x}_3} \varepsilon - \dot{A}_u \quad (32)$$

In order to ensure the stability of the dynamic system, the function $\beta(\tilde{x}_3)$ is designed as

$$\frac{\partial \beta}{\partial \tilde{x}_3} = \rho_2 \varphi'(\tilde{x}_3) \quad (33)$$

$$\varphi'(\tilde{x}_3) = \frac{1}{2} |\tilde{x}_3|^{-\frac{1}{2}} + \gamma$$

Using equation (33), equation (32) is further written as:

$$\dot{\varepsilon} = -\rho_2 \varphi'(\tilde{x}_3) \varepsilon - \dot{A}_u \quad (34)$$

In order to make it easy to express and understand, the system (28) and equation (34) are expressed in the following scalar form, and the stability is proved to ensure that \tilde{x}_3 converge in a finite time.

$$\begin{aligned} \dot{\tilde{x}}_{3i} &= -\rho_1 \varphi(\tilde{x}_{3i}) + \varepsilon_i \\ \dot{\varepsilon}_i &= -\rho_2 \varphi'(\tilde{x}_{3i}) \varepsilon_i - \dot{A}_{ui} \end{aligned} \quad (35)$$

According to Assumption 3, it follows that

$$\dot{A}_{ui} = \vartheta_i(t) \text{sign}(\tilde{x}_{3i}) = \vartheta_i(t) \frac{\varphi(\tilde{x}_{3i})}{|\varphi(\tilde{x}_{3i})|} \quad (36)$$

where $\vartheta_i(t) = \dot{A}_{ui} \text{sign}(\tilde{x}_{3i})$.

Defining a new auxiliary vector $\varsigma_i = [\varphi(\tilde{x}_{3i}) \quad \varepsilon_i]^T$, the dynamic system (35) is rewritten as

$$\dot{\varsigma}_i = \varphi'(\tilde{x}_{3i}) A_i \varsigma_i \quad (37)$$

with $A_i = \begin{bmatrix} -\rho_1 & 1 \\ -\mu_i & -\rho_2 \end{bmatrix}$, $\mu_i = \frac{\vartheta_i(t)}{\varphi'(\tilde{x}_{3i}) |\varphi(\tilde{x}_{3i})|}$.

For the system (37), the Lyapunov function is chosen as

$$V_{li} = \varsigma_i^T P_i \varsigma_i \quad (38)$$

where $P_i = \begin{bmatrix} \eta + 4\varpi^2 & -2\varpi \\ -2\varpi & 1 \end{bmatrix}$ is a symmetric positive definite matrix, η and ϖ are positive numbers.

According to the previous expressions of $\varphi(\tilde{x}_{3i})$ and $\varphi'(\tilde{x}_{3i})$, it follows that

$$\begin{aligned} \varphi'(\tilde{x}_{3i}) |\varphi(\tilde{x}_{3i})| &= \left(\frac{1}{2} |\tilde{x}_{3i}|^{-\frac{1}{2}} + \gamma \right) \left| |\tilde{x}_{3i}|^{\frac{1}{2}} \text{sign}(\tilde{x}_{3i}) + \gamma \tilde{x}_{3i} \right| \\ &= \frac{1}{2} + \frac{3}{2} \gamma |\tilde{x}_{3i}|^{\frac{1}{2}} + \gamma^2 |\tilde{x}_{3i}| \geq \frac{1}{2} \end{aligned} \quad (39)$$

According to the expression of μ_i and equation (39), it can be inferred that $0 < \mu_i < 2\delta_{2i}$. The derivative of the Lyapunov function is written as

$$\begin{aligned} \dot{V}_{li} &= \varsigma_i^T P_i \dot{\varsigma}_i + \varsigma_i^T P_i \dot{\varsigma}_i \\ &= \varphi'(\tilde{x}_{3i}) \varsigma_i^T (A_i^T P_i + P_i A_i) \varsigma_i \\ &= -\varphi'(\tilde{x}_{3i}) \varsigma_i^T Q_i \varsigma_i \end{aligned} \quad (40)$$

Given $Q_i = -(A_i^T P_i + P_i A_i)$, the expression of matrix Q_i is written as

$$Q_i = \begin{bmatrix} Q_{i11} & Q_{i12} \\ Q_{i21} & Q_{i22} \end{bmatrix} \quad (41)$$

with $Q_{i11} = 2\rho_1(\eta + 4\varpi^2) - 4\varpi\mu_i$, $Q_{i22} = 4\varpi + 2\rho_2$, $Q_{i12} = Q_{i21} = \mu_i - 2\varpi\rho_1 - 2\varpi\rho_2 - 4\varpi^2 - \eta$.

In order to make the matrix Q_i a positive definite matrix, the following conditions must be satisfied

$$\begin{aligned} \rho_1 &> \frac{2\varpi\delta_{2i}}{\eta + 4\varpi^2} \\ \rho_2 &> \frac{16\varpi^4 + 8\varpi^2\eta + 16\varpi^2\delta_{2i} + \eta^2 + 4\delta_{2i}^2}{4\eta} \end{aligned} \quad (42)$$

Since P_i and Q_i are positive definite matrices, one obtains

$$\begin{aligned} \lambda_{\min}(P_i) \|\varsigma_i\|^2 &\leq V_{li} = \varsigma_i^T P_i \varsigma_i \leq \lambda_{\max}(P_i) \|\varsigma_i\|^2 \\ \lambda_{\min}(Q_i) \|\varsigma_i\|^2 &\leq \varsigma_i^T Q_i \varsigma_i \leq \lambda_{\max}(Q_i) \|\varsigma_i\|^2 \end{aligned} \quad (43)$$

Using equation (43), equation (40) is further written as

$$\begin{aligned} \dot{V}_{li} &\leq -\lambda_{\min}(Q_i) \varphi'(\tilde{x}_{3i}) \|\varsigma_i\|^2 \\ &\leq -\lambda_{\min}(Q_i) \varphi'(\tilde{x}_{3i}) \frac{V_{li}}{\lambda_{\max}(P_i)} \end{aligned} \quad (44)$$

According to the definition of Euclidean norm, it follows that

$$\|\varsigma_i\|^2 = |\varphi(\tilde{x}_{3i})|^2 + |\varepsilon_i|^2 \geq |\tilde{x}_{3i}| \quad (45)$$

From equation (43) and equation (44), it can be concluded that

$$\|\tilde{x}_{3i}\| \leq \|\varsigma_i\|^2 \leq \frac{V_{li}}{\lambda_{\min}(P_i)} \quad (46)$$

From equation (44), one obtains

$$|\tilde{x}_{3i}|^{-\frac{1}{2}} \geq \left(\frac{V_{li}}{\lambda_{\min}(P_i)} \right)^{\frac{1}{2}} \quad (47)$$

According to equation (46) and equation (49), the derivative of the Lyapunov function \dot{V}_{li} equation can be rewritten as:

$$\begin{aligned} \dot{V}_{li} &\leq -\lambda_{\min}(\mathbf{Q}_i) \left(\frac{1}{2} |\tilde{x}_{3i}|^2 + \gamma \right) \frac{V_{li}}{\lambda_{\max}(\mathbf{P}_i)} \\ &\leq -\frac{\lambda_{\min}(\mathbf{Q}_i)}{2} \left(\frac{V_{li}}{\lambda_{\min}(\mathbf{P}_i)} \right)^{\frac{1}{2}} \frac{V_{li}}{\lambda_{\max}(\mathbf{P}_i)} - \frac{\gamma \lambda_{\min}(\mathbf{Q}_i) V_{li}}{\lambda_{\max}(\mathbf{P}_i)} \quad (48) \\ &= -\tau_{1i} V_{li}^{\frac{1}{2}} - \tau_{2i} V_{li} \end{aligned}$$

where $\tau_{1i} = \frac{\lambda_{\min}(\mathbf{Q}_i) \sqrt{\lambda_{\min}(\mathbf{P}_i)}}{2\lambda_{\max}(\mathbf{P}_i)}$, $\tau_{2i} = \frac{\gamma \lambda_{\min}(\mathbf{Q}_i)}{\lambda_{\max}(\mathbf{P}_i)}$.

If inequality (48) holds, it is concluded that the system (37) is finite time stable.

That is to say, \tilde{x}_3 can converge to 0 within a finite time. From equation (24), it can be inferred that \tilde{x}_3 and s are strictly output passive [24]. Therefore, each subsystem is bounded input bounded output (BIBO) stable. Serial interconnections of BIBO stable system are also BIBO stable. \tilde{x}_3 can converge to 0 within a finite time, then s can also converge to 0. Further, the tracking error \tilde{x}_1 can converge to 0.

To sum up, the Stewart stability platform with the proposed control scheme is stable. Its chematic diagram is given in Figure 5.

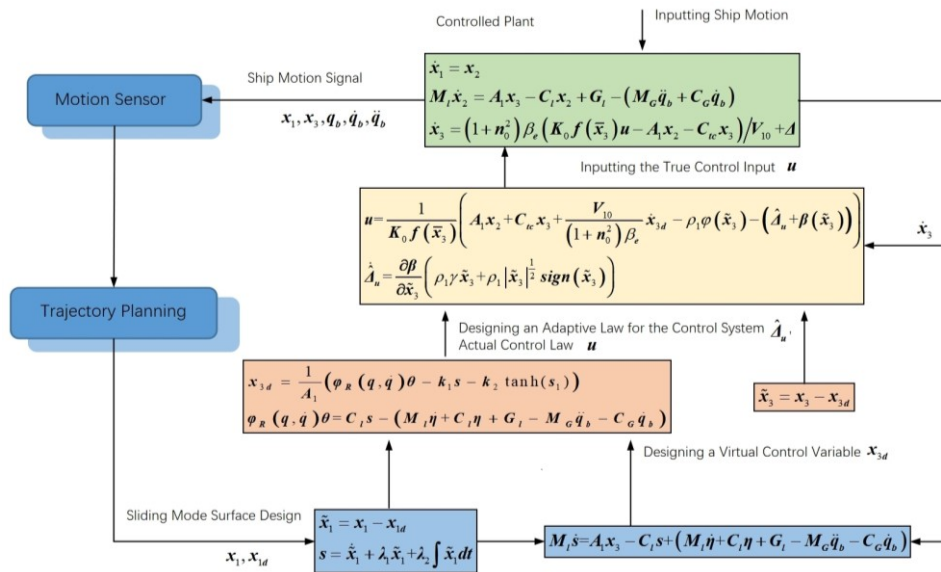


Figure 5: Schematic diagram of adaptive robust control principle

4. Simulation Analysis of Control System

In this section, the simulation model of shipborne stabilization platform control system includes ship trajectory planning, controller design and the mathematical model of the hydraulic actuator. A semi-physical visualization model is constructed according to the parameters of the shipborne stabilization platform (shown in Table 1) (shown in figure 6).

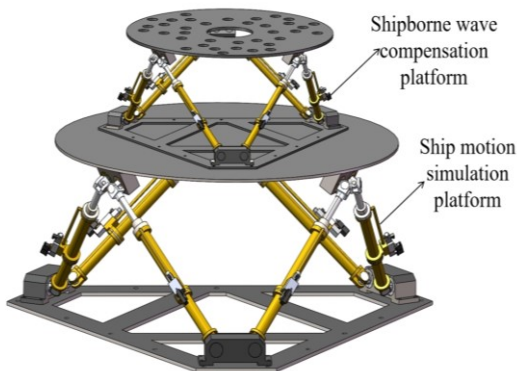


Figure 6: Semi-physical model of ship stability system

Table 1: System parameters of shipborne stabilized platform

parameter	numerical numbe	unit
p_s	28×10^6	Pa
V_N	10	mA
Q_N	250	L/min
β_e	7×10^8	Pa
A_1	0.0031	m ²
w	0.4898	---
c_{id} / c_{ec}	1×10^{-11}	(m ³ /s)/Pa
r_A	1.01	m
d_A	0.15	m
r_B	1.43	m
d_B	0.2	m
l_o	1.65	m
h	1.203	m
p^s	$(0, 0, -0.35)^T$	m
m_p	16000	Kg
I_{pp}	diag(2047, 954.2844)	Kg.m ²

The motion sensor transfers the motion parameters of the ship simulation platform to the controller, and the initial position of the foundation platform under the inertial system and the initial position of the upper platform under the ship conjoined system are marked as $q_p = (0, 0, 0, 0, 0, -h)^T$ and $q_b = (0, 0, 0, 0, 0, 0)^T$, where h is the median height of the platform.

PID control is a commonly used method in engineering, which is simple and effective. The PID control law u_{pi} is as follows

$$u_{pi} = -K_p \tilde{x}_1 - K_I \int_0^1 \tilde{x}_1 dt - K_d \dot{\tilde{x}}_1 \tag{49}$$

Then, a velocity feedforward compensator is added to the above PI controller, and the simulation results are compared. After thorough tuning, a set of controller parameters is selected, as shown in Table 2.

Table 2. Controller parameters of two methods

controller	controller parameters
Adaptive Robust controller	$\lambda_1 = \text{diag}\{20, 20, 20, 20, 20, 20\}$
	$\lambda_2 = \text{diag}\{8 \times 10^{-10}, 8 \times 10^{-10}, 8 \times 10^{-10}, 8 \times 10^{-10}, 8 \times 10^{-10}, 8 \times 10^{-10}\}$
	$k_1 = \text{diag}\{2 \times 10^5, 2 \times 10^5, 2 \times 10^5, 2 \times 10^5, 2 \times 10^5, 2 \times 10^5\}$
	$k_2 = \text{diag}\{1 \times 10^5, 1 \times 10^5, 1 \times 10^5, 1 \times 10^5, 1 \times 10^5, 1 \times 10^5\}$
	$\rho_1 = \text{diag}\{8 \times 10^{-10}, 8 \times 10^{-10}, 8 \times 10^{-10}, 8 \times 10^{-10}, 8 \times 10^{-10}, 8 \times 10^{-10}\}$
PID controller	$K_p = \text{diag}\{100, 100, 100, 100, 100, 100\}$
	$K_I = \text{diag}\{70, 70, 70, 70, 70, 70\}$
	$K_d = \text{diag}\{1 \times 10^{-7}, 1 \times 10^{-7}, 1 \times 10^{-7}, 1 \times 10^{-7}, 1 \times 10^{-7}, 1 \times 10^{-7}\}$

In order to demonstrate the effectiveness of the proposed control strategy, four motion simulation scenarios are used, which are single-degree-of-freedom rolling motion, heave wave spectrum motion and single-degree-of-freedom heave motion. Among them, the single-degree-of-freedom rolling motion scenario: the ship motion input is the sinusoidal motion with a rolling amplitude and frequency of 8 ° and 0.1Hz respectively; heave and rolling wave spectrum motion condition:

since there is no measured ship wave data, the ship heave motion time series (figure 7) and ship roll motion time series (figure 8) are directly used as motion input, and the frequency is concentrated on 0.16Hz~0.4Hz.

Single freedom heave motion condition: the ship motion input is sinusoidal motion with heave amplitude and frequency of 0.2m and 0.5Hz respectively.

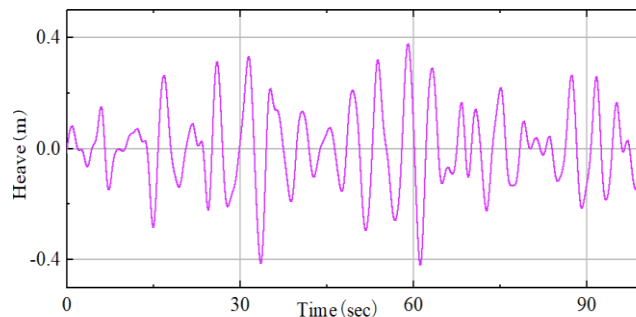


Figure 7: Ship heave motion

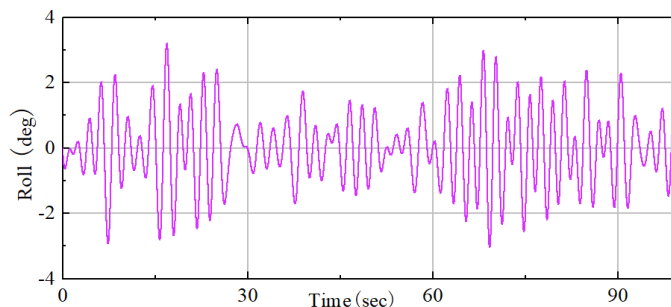


Figure 8: Ship rolling motion

The real results are shown in figures 9 to 11.

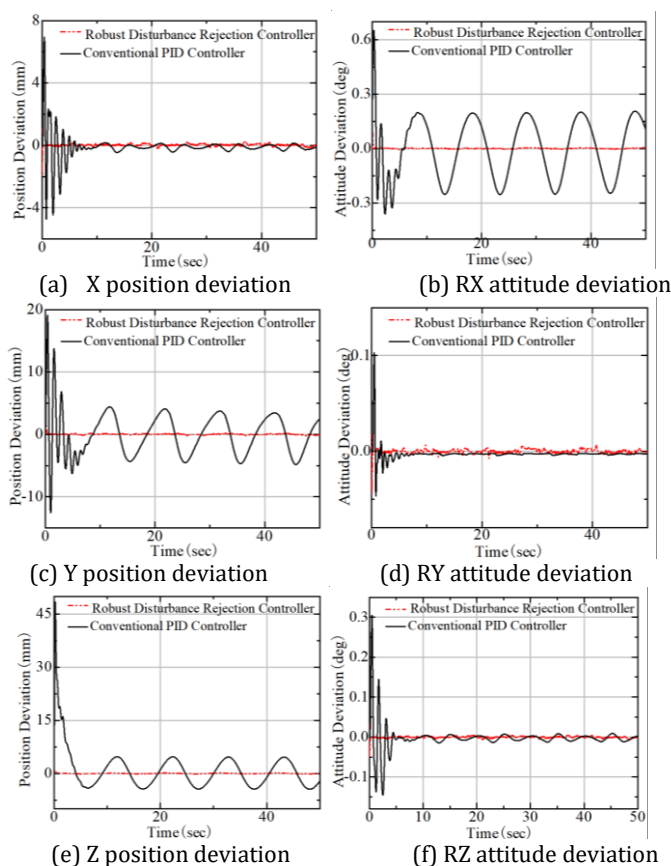


Figure 9: Simulation results of ship rolling motion with single degree of freedom

In order to simulate the actual working conditions, the simulation results of ship motion under 21-ton load are given. Figure 9 shows the pose deviation of the upper platform under the inertial system during the ship's single-freedom rolling motion, in which the red solid line is the result of using the adaptive robust disturbance rejection controller and the black solid line is the result of using the traditional PID controller.

Using the robust disturbance rejection controller, the residual motions of the upper platform is 0.22mm (X direction), 0.19mm (Y direction), 0.15mm (Z direction), 0.0045° (Rx direction), 0.003° (Ry direction) and 0.0038° (Rz direction) respectively.

The residual motion corresponding to the traditional PID controller is 0.16mm (X direction), 4.4mm (Y direction), 4.7mm (Z direction), 0.19° (Rx direction), 0.005° (Ry direction) and 0.017° (Rz direction), respectively.

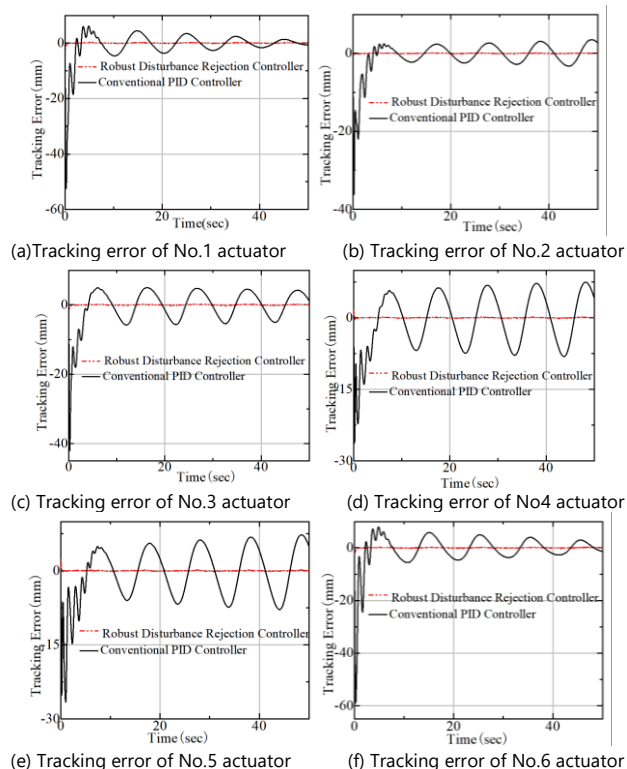


Figure 10: Simulation results of ship rolling motion with single degree of freedom

Figure 10 shows the simulation results of the tracking error between the actual elongation and the expected elongation of the six hydraulic cylinders when the ship has a single degree of freedom rolling motion. Using the adaptive robust disturbance rejection controller, the tracking error amplitudes of each hydraulic cylinder of the stabilized platform are 0.25mm (No. 1), 0.15mm (No. 2), 0.2mm (No. 3), 0.18mm (No. 4), 0.19mm (No. 5) and 0.26mm (No. 6) respectively. The tracking error amplitudes of each hydraulic cylinder corresponding to the traditional PID controller are 4.4mm (No. 1), 2.4mm (No. 2), 4.7mm (No. 3), 6.3mm (No. 4), 5.6mm (No. 5) and 5.8mm (No. 6) respectively.

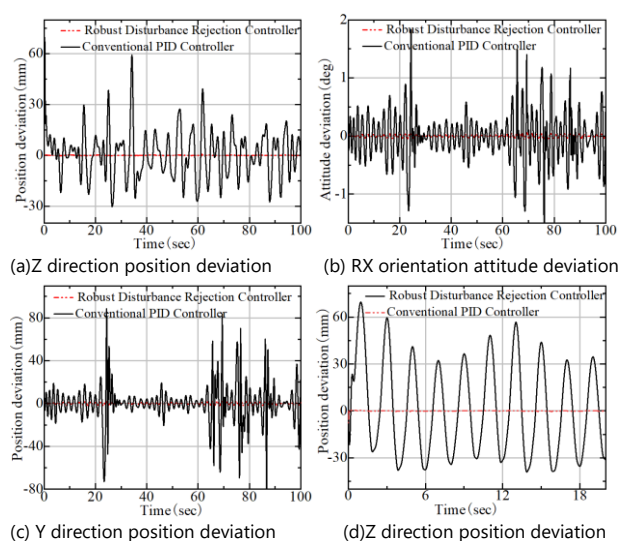


Figure 11: Simulation results of wave spectrum motion and heave motion

Figure 11 (a) shows the simulation results of the heave wave spectrum motion of a ship. Because the deviation of other degrees of freedom is very small, only the position deviation in Z direction is shown here. When using the robust disturbance rejection controller, the residual motion of the upper platform is 0.35mm (Z direction), and the residual motion corresponding to the traditional PID controller is 59mm (Z direction).

Figure 11 (b) (c) shows the simulation results of the rolling wave spectrum motion of a ship. As above, only the attitude deviations in the RX direction and Y direction are shown here. When using the robust disturbance rejection controller, the residual motion of the upper platform is 0.056°(RX direction) and 1.7mm (Y direction), respectively, and the residual motion corresponding to the traditional PID controller is 0.056°(RX direction) and 87mm (Y direction).

Figure 11 (d) shows the simulation results of single-degree-of-freedom heave motion. As above, only the Z-direction position deviation is shown here. When using the adaptive robust disturbance rejection controller, the residual motion of the upper platform is 0.38mm (Z-direction), and the residual motion

corresponding to the traditional PID controller is 56mm (Z-direction).

Through the above simulation results, it can be seen that the proposed adaptive robust disturbance rejection controller has better control performance than the traditional PID controller. Especially when facing the high frequency motion of ocean wave spectrum, the control effect of traditional PID controller is poor, which is much lower than that of robust disturbance rejection controller. The reason is that the proposed backstepping adaptive robust disturbance rejection control strategy includes dynamic compensation. Dynamic compensation is used to compensate the disturbance force of ship motion under heavy load. In addition, the inertia matrix is included in the dynamic compensation term, which makes the backstepping adaptive robust disturbance rejection control strategy has strong robustness to systems with different dynamic characteristics, so it can further improve the performance of wave compensation.

5. Conclusions

In this paper, the state equation of parallel 6-DOF ship stabilized platform system is constructed, and the controller is designed by recursive backstepping method. Combined with continuous sliding mode and a novel intrusion-invariant robust adaptive law, an adaptive robust disturbance rejection control strategy is designed to improve the anti-jamming ability and control accuracy of the stable platform. The stability of the system is proved by using Lyapunov function theory. The control system model is built, and the performance of 6-DOF parallel ship stabilization platform under the disturbance of ship motion under different control algorithms is simulated and analyzed. The simulation results show that the control method proposed in this paper can improve the tracking performance and robustness, and is more suitable for the control of six-degree-of-freedom parallel stable platform under complex sea conditions.

Acknowledgments

This research was supported in part by the Foundation of the Education Department of Henan Province (No.23A460006), the Foundation of Henan University of Technology (No. 2021BS071), the Key Scientific and Technological Research Projects in Henan Province (No. 242102240039).

References

- [1]Sun, H., Gao, S., Liu, J., et al. (2022). Research on Comprehensive Benefits and Reasonable Selection of Marine Resources Development Types. *Open Geosciences*, 14(1), 141-150.

- [2] Sosa-Méndez, D., Lugo-González, E., Arias-Montiel, M., & García-García, R. A. (2017). ADAMS-MATLAB Co-simulation for Kinematics, Dynamics, and Control of the Stewart-Gough Platform. *International Journal of Advanced Robotic Systems*, 14(4).
- [3] Dumlu, A., Erentürk, K., Kaleli, A., & Ayten, K. K. (2017). A Comparative Study of Two Model-Based Control Techniques for the Industrial Manipulator. *Robotica*, 35(10), 2036-2055.
- [4] Hu, Y. (2015). Research on Key Technologies of Design and Control of Parallel Wave Compensation System with Six DOFs [D]. Changsha: National University of Defense Technology.
- [5] Salzman, D. (2010). Development of the Access System for Offshore Wind Turbines (Ph.D. thesis). Delft University of Technology.
- [6] Meng, Q., Zhang, T., He, J. F., Song, J. Y., & Yuan, C. Y. (2014). Fault-Tolerant Control of Uncertain Stewart Platform Under Loss of Actuator Effectiveness. *Proceedings of the Institution of Mechanical Engineers, Part C: Journal of Mechanical Engineering Science*, 228(8), 1286-1298.
- [7] Lafmejani, A. S., Masouleh, M. T., & Kalhor, A. (2018). Trajectory Tracking Control of a Pneumatically Actuated 6-DOF Gough-Stewart Parallel Robot Using Backstepping-Sliding Mode Controller and Geometry-Based Quasi Forward Kinematic Method. *Robotics and Computer-Integrated Manufacturing*, 54, 96-114.
- [8] Velasco, J., Calvo, I., Barambones, O., Venegas, P., & Napole, C. (2020). Experimental Validation of a Sliding Mode Control for a Stewart Platform Used in Aerospace Inspection Applications. *Mathematics*, 8(11), 2051.
- [9] Keshtkar, S., Poznyak, A. S., Hernandez, E., & Oropeza, A. (2017). Adaptive Sliding-Mode Controller Based on the "Super-Twist" State Observer for Control of the Stewart Platform. *Automation and Remote Control*, 78, 1218-1233.
- [10] Xie, B., & Dai, S. (2022). Robust Terminal Sliding Mode Control on SE (3) for Gough-Stewart Flight Simulator Motion Platform with Payload Uncertainty. *Electronics*, 11(5), 814.
- [11] Eftekhari, M., Eftekhari, M., & Karimpour, H. (2015). Neuro-Fuzzy Adaptive Control of a Revolute Stewart Platform Carrying Payloads of Unknown Inertia. *Robotica*, 33(9), 2001-2024.
- [12] Jishnu, A. K., Chauhan, D. K., & Vundavilli, P. R. (2022). Design of Neural Network-Based Adaptive Inverse Dynamics Controller for Motion Control of Stewart Platform. *International Journal of Computational Methods*, 19(08), 2142010.
- [13] Chen, S. H., & Fu, L. C. (2015). Observer-Based Backstepping Control of a 6-DOF Parallel Hydraulic Manipulator. *Control Engineering Practice*, 36, 100-112.
- [14] Yadavari, H., Tavakol Aghaei, V., & İközöğlü, S. (2023). Deep Reinforcement Learning-Based Control of Stewart Platform with Parametric Simulation in ROS and Gazebo. *Journal of Mechanisms and Robotics*, 15(3), 035001.
- [15] Dumitriu, D. N., Mărgăritescu, M., & Rolea, A. M. E. (2017). Direct Dynamics of Gough-Stewart Hexapod Platforms Using the Redundant Parameterisation of Rotations by Full Rotation Matrices. *International Journal of Mechatronics and Applied Mechanics*, 1(1), 159-167.
- [16] Cai, Y., Zheng, S., Liu, W., Qu, Z., & Han, J. (2020). Model Analysis and Modified Control Method of Ship-Mounted Stewart Platforms for Wave Compensation. *IEEE Access*, 9, 4505-4517.
- [17] Qiang, H., Jin, S., Feng, X., et al. (2020). Model Predictive Control of a Shipborne Hydraulic Parallel Stabilized Platform Based on Ship Motion Prediction. *IEEE Access*, 8, 181880-181892.
- [18] Chen, W., Wang, S., Li, J., Lin, C., Yang, Y., Ren, A., ... & Gao, F. (2023). An ADRC-Based Triple-Loop Control Strategy of Ship-Mounted Stewart Platform for Six-DOF Wave Compensation. *Mechanism and Machine Theory*, 184, 105289.
- [19] Chen, W., Wen, Y., Tong, X., Lin, C., Li, J., Wang, S., ... & Gao, F. (2023). Dynamics Modeling and Modal Space Control Strategy of Ship-Borne Stewart Platform for Wave Compensation. *Journal of Mechanisms and Robotics*, 15(4), 041015.
- [20] Cai, Y., Zheng, S., Liu, W., et al. (2021). Sliding-Mode Control of Ship-Mounted Stewart Platforms for Wave Compensation Using Velocity Feedforward. *Ocean Engineering*, 236, 109477.
- [21] Cai Y, Zheng S, Liu W, et al. (2021). Adaptive robust dual-loop control scheme of ship-mounted Stewart platforms for wave compensation. *Mechanism and Machine Theory*, 164, 104406.
- [22] Jing, C., Xu, H., & Niu, X. (2019). Adaptive Sliding Mode Disturbance Rejection Control with Prescribed Performance for Robotic Manipulators. *ISA Transactions*, 91, 41-51.
- [23] Zheng, Z., Zhang, H., & Vo, D. T. (2020). Analysis of model-free sliding mode control of permanent magnet synchronous motor. *International Journal of Mechatronics and Applied Mechanics*, 2(8), 217-224.
- [24] Kim, W., Won, D., Shin, D., & Chung, C. C. (2012). Output Feedback Nonlinear Control for Electro-Hydraulic Systems. *Mechatronics*, 22(6), 766-777.